SAND2008-7844C

Sensor Selection for Wind Turbine State Estimation*

Jonathan Berg† Keith Miller‡

Abstract

This paper presents a sensor selection study for efficient estimation of wind turbine rotor state and wind-induced load state. Sensor type and placement is simulated on a finite element model of a turbine blade. The Kalman filter is utilized to estimate the turbine state and gage the effect of sensor noise level. Estimation of wind-load state is accomplished with an extended Kalman filter using only a small set of measurements.

Nomenclature

$\mathbf{A}$	continuous-time state matrix
$\mathbf{B}$	continuous-time input matrix
$\mathbf{C}$	damping matrix
$\mathbf{G}$	continuous-time process noise input matrix
$\mathbf{H}$	output matrix
$\mathbf{I}$	identity matrix
$\mathbf{K}$	stiffness matrix or Kalman gain matrix
$\mathbf{M}$	mass matrix
$\mathbf{P}$	estimate error covariance matrix
$\mathbf{Q}$	process noise covariance matrix
$\mathbf{q}$	input force vector
$\mathbf{R}$	measurement noise covariance matrix
$\mathbf{u}$	vector of nodal displacements (both transverse and rotational)
$\mathbf{v}$	measurement noise vector
$\mathbf{w}$	process noise vector
$\mathbf{x}$	state vector

*Work in partial fulfillment of completion of a Masters of Science Degree in Mechanical Engineering, NMT. Work is sponsored by Sandia National Laboratories, under US Department of Energy Prime Contract, DE-AC04-94AL85000. Work supervised by Mr. Dale Berg, Principal Member of Technical Staff, Sandia National Laboratories.

†Graduate Student of Mechanical Engineering Department, New Mexico Institute of Mining and Technology, Socorro, NM 87801, jberg@nmt.edu

‡Associate Professor of Mechanical Engineering Department, New Mexico Institute of Mining and Technology, Socorro, NM 87801

$\hat{\mathbf{x}}$	estimate state vector
$\tilde{\mathbf{y}}$	measured output vector
$\mathbf{\Phi}$	discrete-time state matrix
$\mathbf{\Gamma}$	discrete-time input matrix
$\mathbf{\Upsilon}$	discrete-time process noise input matrix
$[\quad]^T$	matrix transpose
$[\quad]^{-1}$	matrix inverse
IEC	International Electrotechnical Commission
NTM	normal turbulence model
RMS	root-mean-square

1 Introduction

To enable advanced control schemes for wind energy conversion systems, the turbine state will need to be estimated from a small set of measurements. To make full use of active aerodynamic devices, it will likely be necessary to estimate the distributed wind load and full blade state. Both of these advances could contribute greatly to the efficiency and longevity of future wind turbines. Such considerations have motivated this investigation of state and input estimation via the Kalman filter.

The blade model was formulated using simple beam elements from Euler-Bernoulli beam theory. A number of sensor types, including strain, displacement, and velocity, were simulated with an appropriate transform of the state vector. In this fashion, various combinations of sensor type, number, and placement were evaluated with regard to the estimation error. In addition, the structure of the Kalman filter provided a way of gaging the effects of sensor noise level.

Estimation of the input forces was accomplished by extending the Kalman filter's state vector to include the forces themselves. Knowledge of the dynamics governing the input forces is not required. Rather, an accurate structural dynamics model provides the necessary information to infer the applied forces from the structural response.

A brief survey of estimation research pertaining to wind turbines and input estimation is now given. Input estimation of beam structures has been studied by C.K. Ma [1] using the method of Tuan [2], and estimation of effective wind speed has been explored by X. Ma [3] and Østergaard [4]. Boukhezzar [5] uses the Kalman filter to estimate aerodynamic torque from the rotor speed and also demonstrates its application in an "aerodynamic torque feedforward" controller and a "nonlinear dynamic state feedback" controller. Ehlers [6] looks at sensor selection and state estimation of the blade, tower, drive shaft, and wind speed. The concept of "distance to unobservability" is used to evaluate sensor combinations.

2 Model Formulation

A 1.5MW wind turbine blade was selected for study. The WindPACT Baseline model packaged with FAST [7] provided the property definitions needed to create a simple finite-element beam model of the 35 meter long blade. Only the flapwise (primary) direction of bending was modeled. The system equation is

$$\mathbf{M}\ddot{\mathbf{u}}(t) + \mathbf{C}\dot{\mathbf{u}}(t) + \mathbf{K}\mathbf{u}(t) = \mathbf{q}(t) \tag{1}$$

where the vector $\mathbf{u}$ contains the transverse displacement u_{yi} and rotation θ_{zi} at each node. The mass and stiffness matrices were formed using finite elements derived from Euler-Bernoulli beam theory, while the damping matrix was defined using modal damping with a damping ratio of 0.04 for each mode. Input loads $\mathbf{q}$ were assumed to consist of transverse loads only and no applied bending moments.

For a beam element with length h, linear density ρ, and flexural stiffness property EI, the element mass and stiffness matrices are given by

$$\mathbf{m} = \frac{\rho h}{420}\begin{bmatrix} 156 & 22h & 54 & -13h \\ 22h & 4h^2 & 13h & -3h^2 \\ 54 & 13h & 156 & -22h \\ -13h & -3h^2 & -22h & 4h^2 \end{bmatrix} \tag{2}$$

$$\mathbf{k} = \frac{EI}{h^3}\begin{bmatrix} 12 & 6h & -12 & 6h \\ 6h & 4h^2 & -6h & 2h^2 \\ -12 & -6h & 12 & -6h \\ 6h & 2h^2 & -6h & 4h^2 \end{bmatrix} \tag{3}$$

where the element degrees-of-freedom are $\mathbf{u_e} = \begin{bmatrix} u_{y1} & \theta_{z1} & u_{y2} & \theta_{z2} \end{bmatrix}^T$.

Resonant mode frequencies of the beam were calculated using a model with 15 elements of equal length. The first five frequencies are shown in Table 2, and illustrations of the beam and a few of its mode shapes are given in Figure 1.

To convert the model into state-space form, the state vector was defined to include the nodal degrees-of-freedom and their time derivatives. It was assumed that process noise $\mathbf{w}$ appears as noise on the input forces. The state-space model

Table 2: Blade flapwise resonant mode frequencies.

Mode	Frequency (Hz)	Damping ratio
1	1.25	0.04
2	3.75	0.04
3	8.24	0.04
4	15.08	0.04
5	23.42	0.04

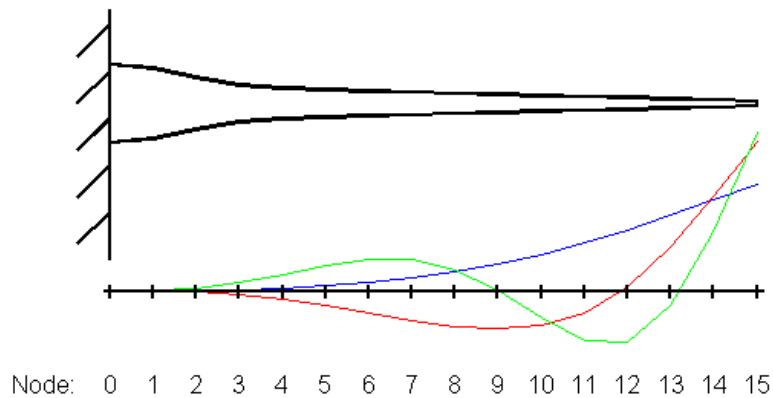

Figure 1: Tapered beam representing a 1.5MW turbine blade. First three resonant modes are given.

is then given by

$$\dot{\mathbf{x}}(t) = \begin{bmatrix} \mathbf{0} & \mathbf{I} \\ -\mathbf{M}^{-1}\mathbf{K} & -\mathbf{M}^{-1}\mathbf{C} \end{bmatrix} \mathbf{x}(t) + \begin{bmatrix} \mathbf{0} \\ \mathbf{M}^{-1} \end{bmatrix} \mathbf{q}(t) + \begin{bmatrix} \mathbf{0} \\ \mathbf{M}^{-1} \end{bmatrix} \mathbf{w}(t) \tag{4a}$$

$$\tilde{\mathbf{y}}(t) = \mathbf{H}\mathbf{x}(t) + \mathbf{v}(t) \tag{4b}$$

where $\mathbf{x} = \begin{bmatrix} \mathbf{u}^T & \dot{\mathbf{u}}^T \end{bmatrix}^T$ and the form of $\mathbf{H}$ depends on the measurement system.

3 The Kalman Filter

The Kalman filter is a recursive filter that can be used to estimate the complete state of a dynamic system. The filter definition requires a system model, an appropriate set of measurements, knowledge of the input, and the covariance matrices of the process noise and measurement noise. The system model is expressed in state-space form as a set of first-order differential equations.

$$\dot{\mathbf{x}}(t) = \mathbf{A}\mathbf{x}(t) + \mathbf{B}\mathbf{q}(t) + \mathbf{G}\mathbf{w}(t) \tag{5a}$$

$$\tilde{\mathbf{y}}(t) = \mathbf{H}\mathbf{x}(t) + \mathbf{v}(t) \tag{5b}$$

In the filter formulation, noise vectors $\mathbf{w}$ and $\mathbf{v}$ are assumed to be zero-mean Gaussian white-noise processes, such that

$$\begin{aligned} E\left\{\mathbf{w}(t)\mathbf{w}^T(\tau)\right\} &= \mathbf{Q}(t)\delta(t-\tau) \\ E\left\{\mathbf{v}(t)\mathbf{v}^T(\tau)\right\} &= \mathbf{R}(t)\delta(t-\tau) \\ E\left\{\mathbf{v}(t)\mathbf{w}^T(\tau)\right\} &= 0 \end{aligned} \tag{6}$$

To simplify implementation of the system model and Kalman filter, the continuous-time system model can be converted to discrete-time. Also, covariance matrices $\mathbf{R}$ and $\mathbf{Q}$ are assumed to be constant with respect to time.

$$\mathbf{x}_{k+1} = \mathbf{\Phi}\mathbf{x}_k + \mathbf{\Gamma}\mathbf{q}_k + \mathbf{\Upsilon}\mathbf{w}_k, \quad \mathbf{w}_k \sim N(\mathbf{0}, \mathbf{Q}) \tag{7a}$$

$$\tilde{\mathbf{y}}_k = \mathbf{H}\mathbf{x}_k + \mathbf{v}_k, \quad \mathbf{v}_k \sim N(\mathbf{0}, \mathbf{R}) \tag{7b}$$

The discrete-time Kalman filter as presented in [8] is given by

$$\hat{\mathbf{x}}_{k+1} = \mathbf{\Phi}\hat{\mathbf{x}}_k + \mathbf{\Gamma}\mathbf{q}_k + \mathbf{\Phi}\mathbf{K}_k[\tilde{\mathbf{y}}_k - \mathbf{H}\hat{\mathbf{x}}_k] \tag{8a}$$

$$\mathbf{K}_k = \mathbf{P}_k\mathbf{H}^T[\mathbf{H}\mathbf{P}_k\mathbf{H}^T + \mathbf{R}]^{-1} \tag{8b}$$

$$\mathbf{P}_{k+1} = \mathbf{\Phi}\mathbf{P}_k\mathbf{\Phi}^T - \mathbf{\Phi}\mathbf{K}_k\mathbf{H}\mathbf{P}_k\mathbf{\Phi}^T + \mathbf{\Upsilon}\mathbf{Q}\mathbf{\Upsilon}^T \tag{8c}$$

This recursive algorithm produces $\hat{\mathbf{x}}$, the estimate of the state vector at each time step. The time-varying matrix $\mathbf{K}$ is known as the Kalman gain matrix, and it serves to correct the state estimate based upon the vector of measured outputs $\tilde{\mathbf{y}}$. The time-varying matrix $\mathbf{P}$ is the estimate error covariance.

To estimate the input vector $\mathbf{q}$, one approach is to redesign the Kalman filter such that the input vector is included in the state vector [5]. However, the dynamics relating $\dot{\mathbf{q}}$ to the state vector are likely unknown. This lack of knowledge can be modeled by writing zeros in the state transition matrix and accounting for the error with a noise vector $\mathbf{z}$ having large signal variance.

$$\begin{bmatrix}\mathbf{x}_{k+1}\\ \mathbf{q}_{k+1}\end{bmatrix} = \begin{bmatrix}\mathbf{\Phi} & \mathbf{\Gamma}\\ \mathbf{0} & \mathbf{0}\end{bmatrix}\begin{bmatrix}\mathbf{x}_k\\ \mathbf{q}_k\end{bmatrix} + \begin{bmatrix}\mathbf{\Upsilon} & \mathbf{0}\\ \mathbf{0} & \mathbf{I}\end{bmatrix}\begin{bmatrix}\mathbf{w}_k\\ \mathbf{z}_k\end{bmatrix}, \quad \begin{bmatrix}\mathbf{w}_k\\ \mathbf{z}_k\end{bmatrix} \sim N\left(\mathbf{0}, \begin{bmatrix}\mathbf{Q_w} & \mathbf{0}\\ \mathbf{0} & \mathbf{Q_z}\end{bmatrix}\right) \tag{9a}$$

$$\tilde{\mathbf{y}}_k = \begin{bmatrix}\mathbf{H} & \mathbf{0}\end{bmatrix}\begin{bmatrix}\mathbf{x}_k\\ \mathbf{q}_k\end{bmatrix} + \mathbf{v}_k, \quad \mathbf{v}_k \sim N(\mathbf{0}, \mathbf{R}) \tag{9b}$$

Thus, the extended Kalman filter for input estimation uses the following alterations to Equation Set 8.

$$\begin{gathered}\mathbf{\Phi}_{new} = \begin{bmatrix}\mathbf{\Phi} & \mathbf{\Gamma}\\ \mathbf{0} & \mathbf{0}\end{bmatrix}, \quad \mathbf{\Gamma}_{new} = \mathbf{0}, \quad \mathbf{\Upsilon}_{new} = \begin{bmatrix}\mathbf{\Upsilon} & \mathbf{0}\\ \mathbf{0} & \mathbf{I}\end{bmatrix},\\ \mathbf{Q}_{new} = \begin{bmatrix}\mathbf{Q_w} & \mathbf{0}\\ \mathbf{0} & \mathbf{Q_z}\end{bmatrix}, \quad \mathbf{H}_{new} = \begin{bmatrix}\mathbf{H} & \mathbf{0}\end{bmatrix}\end{gathered} \tag{10}$$

4 Simulation Setup and Results

Turbulent wind was selected as the loading condition so that the response would be similar to that seen in the field. An IEC normal turbulence model with 9 m/s average wind speed was generated using TurbSim [9] and applied to the WindPACT Baseline 1.5 MW model in FAST [7]. A sample of the resulting aerodynamic forces normal to the rotor plane are given in Figure 2 (these forces are approximately in the flapwise direction for most of the blade span). The mean load and two-standard-deviation bounds are shown in Figure 3.

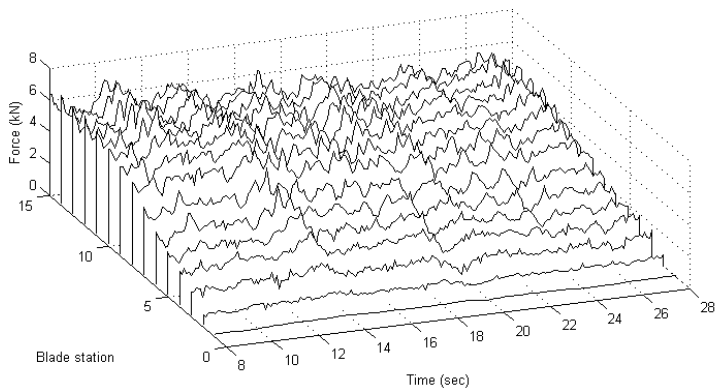

Figure 2: Forces resulting from IEC NTM with 9 m/s average wind speed.

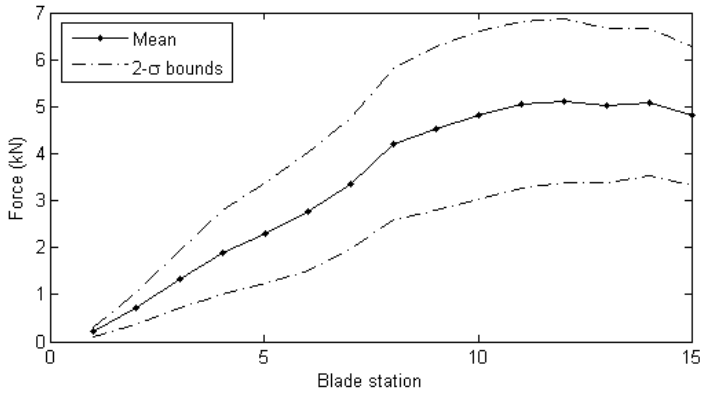

Figure 3: The mean nodal loads and 2-σ bounds for a simulation lasting 120 seconds.

4.1 Sensor Study

The Kalman Filter assumes that the input vector is known at each time step and any uncertainty is modeled by the noise vector $\mathbf{w}$. In this section, a moving average zero-phase filter with one of two window sizes was applied to the input forces to obtain different amounts of uncertainty in the knowledge of the input vector. A small window results in low uncertainty. The original input was applied to the system but the filtered input was applied to the Kalman state observer. $\mathbf{Q}$, the covariance of $\mathbf{w}$, was taken to be the covariance of $(\mathbf{q} - \mathbf{q}_{filt})$. Figure 4 uses surface plots to visualize $\mathbf{Q}$ for window sizes of 20 and 200 (0.1- and 1-second averages).

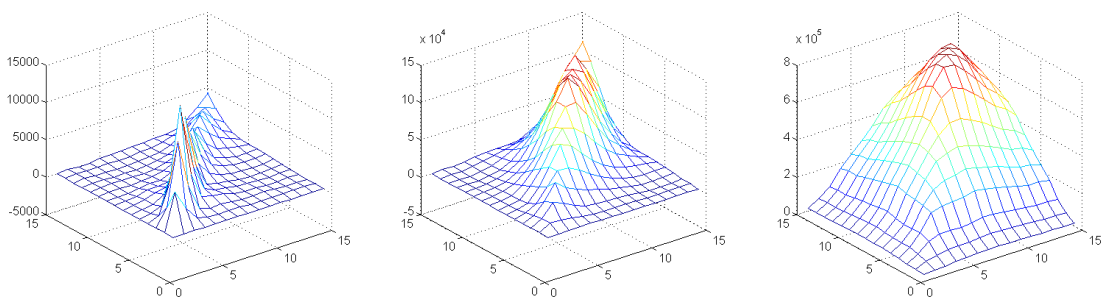

Figure 4: Process noise covariance $\mathbf{Q}$ with moving average window size 20 (left) and 200 (center). Right: covariance of $\mathbf{q}$ (window size is entire time history).

The definition of percent error given in Equation 11 was used to quantify the estimation error [1]. It is essentially the RMS error divided by the RMS true signal. "Blade-average deflection state percent error" was defined as the average of all nodal transverse displacement errors. "Blade-average velocity state percent error" was likewise defined for the errors in transverse rate-of-displacement.

$$e_i = \frac{\sqrt{\sum_{\text{all } k}(\hat{x}_i(k) - x_i(k))^2}}{\sqrt{\sum_{\text{all } k}(x_i(k))^2}} \times 100 \tag{11}$$

The following sensor types and placements were investigated. Sensor signal variance is R in each case ($\mathbf{R} = R \times \mathbf{I}$ for multiple sensors).

- A single displacement sensor at node 7, 9, 11, or 15. Repeated for velocity sensor.
- A pair of displacement sensors at nodes 7 and 15. Repeated for velocity sensor.
- A single strain sensor at node 1 or 7.
- A pair of strain sensors at nodes 1 and 7.

Figures 5 through 7 present the results with the $\mathbf{q}_{filt}$ window size set to 20. Note that, even with very good knowledge of the force input, the velocity state-variable estimation error can be as great as 24%. However, the beam's deflection state is known with error below 1%. Because deflection and velocity are higher at the tip, more measurement noise tolerance is seen as these sensors move toward the tip. Comparing displacement- and velocity-type sensors, the velocity sensors achieve the same error levels at higher sensor noise levels. Given that the RMS tip deflection was around 2 meters and the RMS tip velocity was around 1 m/s, the higher noise tolerance cannot be explained by differences in signal amplitude. Rather, the filter is better able to utilize the velocity information. For the most part, the character of strain sensors is similar to that of displacement sensors.

Figures 8 through 10 present the results with the window size set to 200. At this level of input uncertainty, deflection state error now extends up to 7%, which is still a rather good estimate of the beam's deflection. Velocity state estimation error has increased to the 40-100% range. The advantage of velocity measurements over displacement measurements is once again observed.

Comparing the results from the low and high input-uncertainty groups, curves in the later group are shifted to the right. It should be noted that the *relative* size of $\mathbf{R}$ to $\mathbf{Q}$ tends to control the Kalman filter's performance. Thus, it was expected that the shift to the right would occur because the magnitude of $\mathbf{Q}$ has increased with increasing input uncertainty. However, it may be permissible to venture a physical interpretation of the effect: as the system model uncertainty increases, the filter is more willing to utilize noisy measurements.

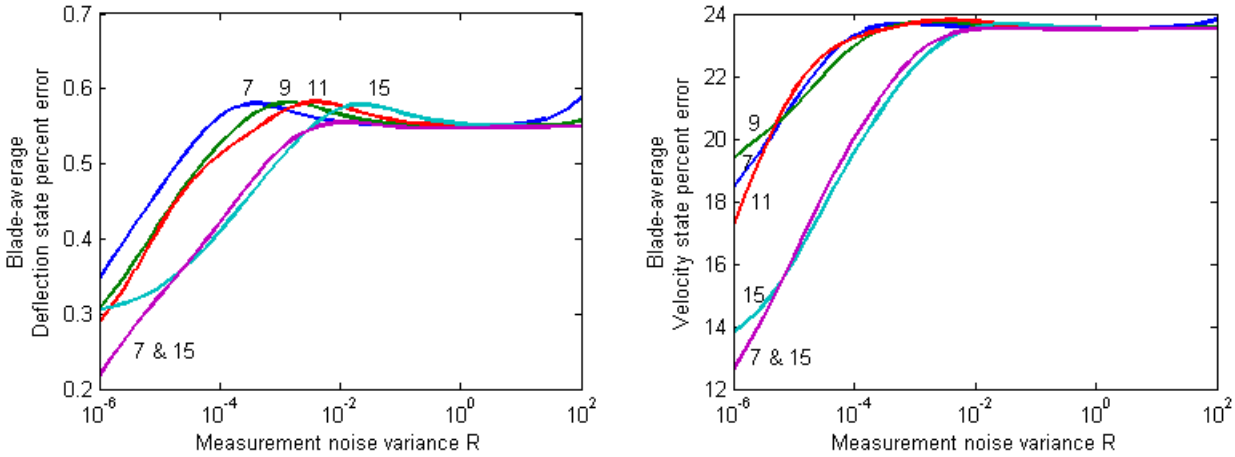

Figure 5: Estimation percent error resulting from a displacement sensor at the specified nodes. Moving average window size is 20.

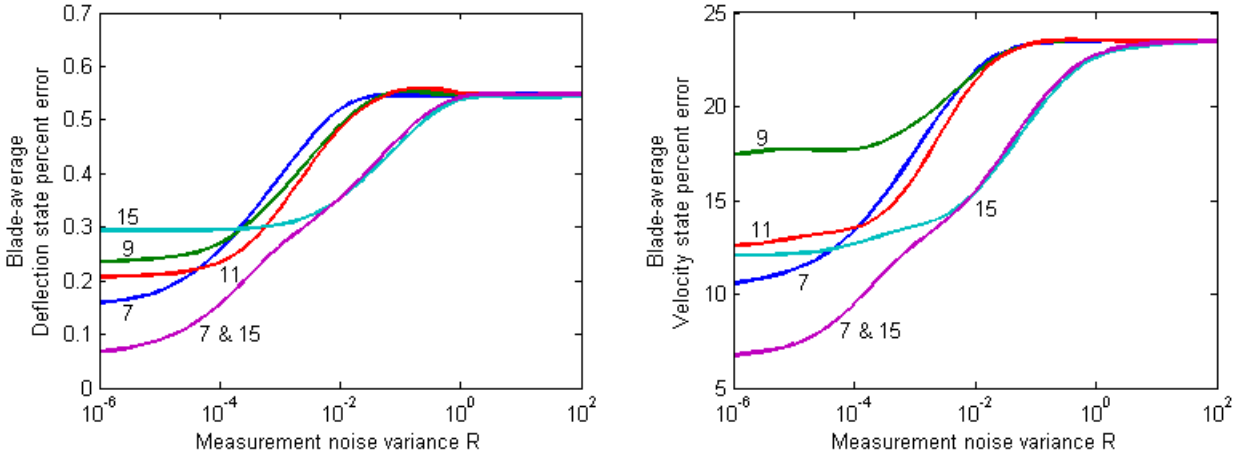

Figure 6: Estimation percent error resulting from a velocity sensor at the specified nodes. Moving average window size is 20.

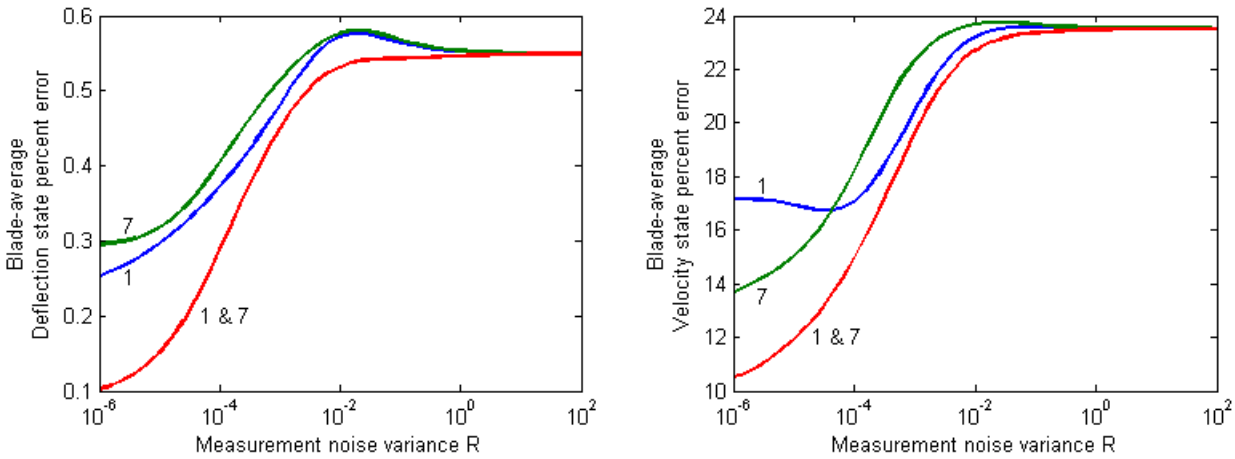

Figure 7: Estimation percent error resulting from a strain sensor at the specified nodes. Moving average window size is 20.

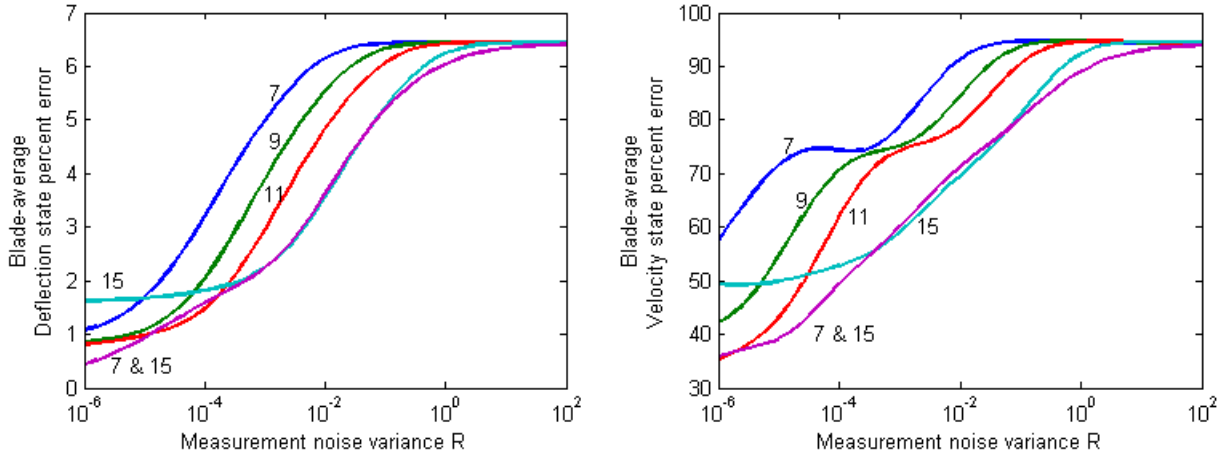

Figure 8: Estimation percent error resulting from a displacement sensor at the specified nodes. Moving average window size is 200.

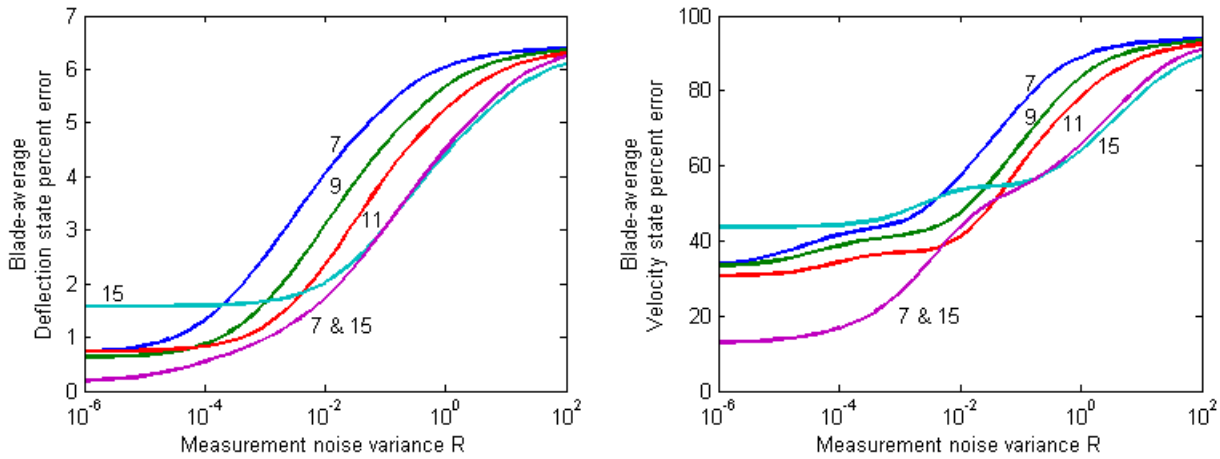

Figure 9: Estimation percent error resulting from a velocity sensor at the specified nodes. Moving average window size is 200.

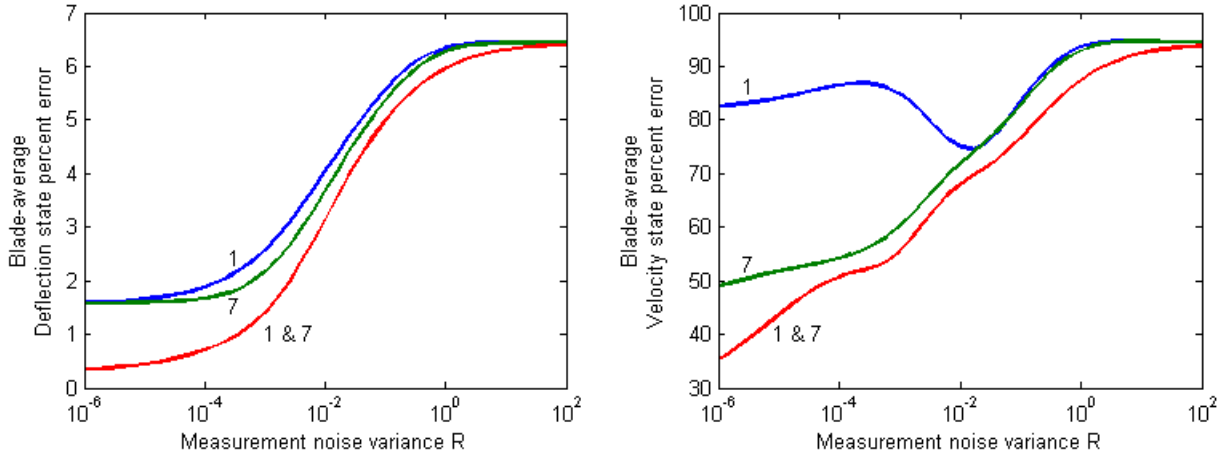

Figure 10: Estimation percent error resulting from a strain sensor at the specified nodes. Moving average window size is 200.

4.2 Force Estimation

The extended Kalman filter was tested with the following configuration. Process noise covariance $\mathbf{Q_w}$ was set equal to the covariance of the entire force time history, and the covariance of the extended states was chosen to be $\mathbf{Q_z} = 10^8 \times \mathbf{I}$. The measurement system was defined by displacement sensors at nodes 7 and 15 with sensor noise covariance equal to $\mathbf{R} = 10^{-2} \times \mathbf{I}$. Force estimation results are given in Figure 11. Percent error is about 30% at the blade root and decreases to about 10% for nodes 7 through 15.

To see if more sensors would improve the estimation accuracy, all nodes were given displacement sensors. With the other filter parameters kept the same, the result is actually quite opposite from expectations. Maximum percent error is 50%, outer portion of blade is at 15% error, and the force estimate occasionally takes on strange shapes (see Figure 12). At this point, the main conclusion is that the choice of sensors and Kalman filter parameters $\mathbf{Q_w}$, $\mathbf{Q_z}$, and $\mathbf{R}$ interact in complicated ways.

5 Discussion and Conclusions

The relationship of estimation error to sensor type, placement, and noise level has been investigated. It should be noted that there is not necessarily a one-to-one correspondence between $\mathbf{R}$ and the sensor noise allowed in the physical system. The Kalman filter is designed to produce minimum-variance optimal estimates when $\mathbf{R}$ is exactly equal to the measurement covariance. In practice, however, $\mathbf{R}$ and $\mathbf{Q}$ tend to be used as "tuning knobs" which control the performance of the filter. The curves in Figures 5 through 10 do provide a sense of the required measurement precision (relative to the model uncertainty) and what improvements are possible with low-noise sensors. In this analysis, velocity-type measurements show an advantage over displacement-type measurements, but it is yet to be seen whether this effect also occurs with force estimation. Future work will also investigate acceleration as a measurement possibility.

An extended Kalman filter was successfully utilized to estimate input forces using only two displacement sensors. The filter tracks the mean force level while filtering out high frequency variations. Future work will explore other measurements sets and determine appropriate selections for the Kalman filter parameters.

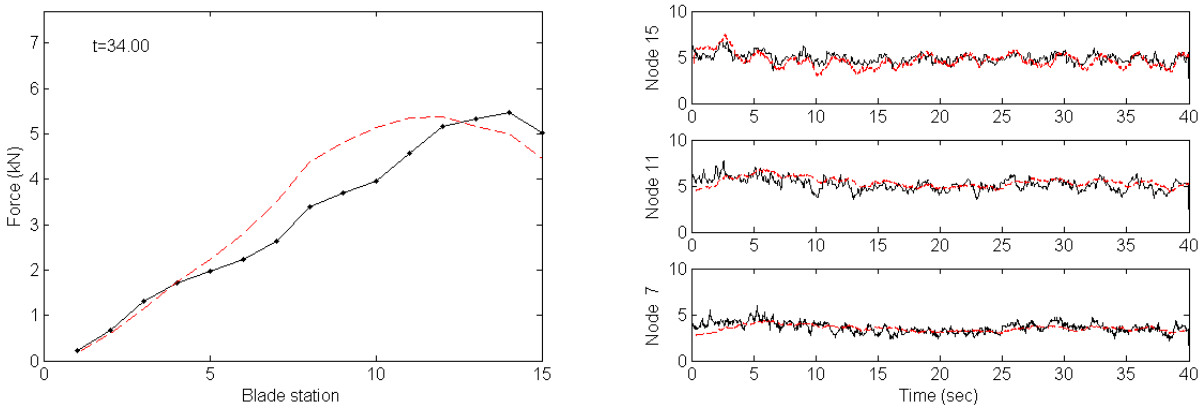

Figure 11: Displacement sensors at nodes 7 and 15. Black solid lines are true forces. Red dashed lines are force estimates. Left: snapshot in time. Right: time histories of a few nodal forces.

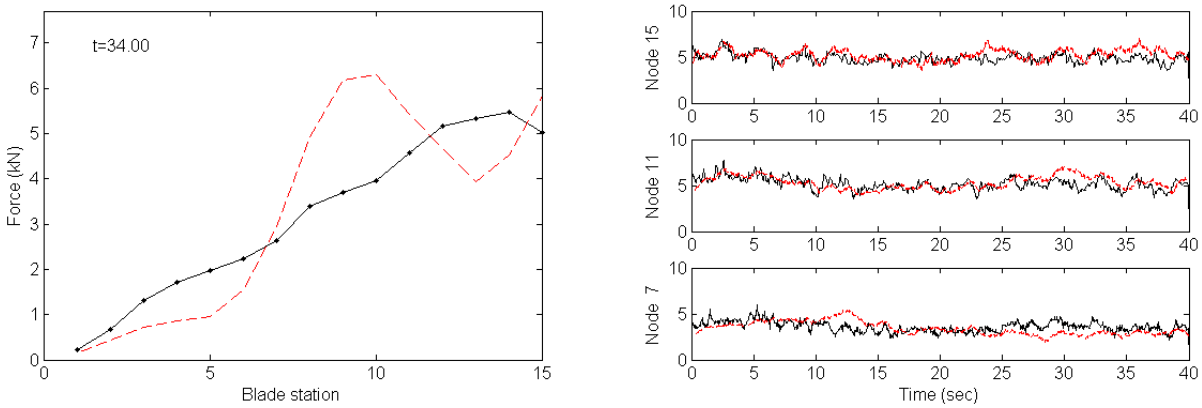

Figure 12: Displacement sensors at all nodes. Black solid lines are true forces. Red dashed lines are force estimates. Left: snapshot in time. Right: time histories of a few nodal forces.

References

[1] C.K. Ma, J.M. Chang, and D.C. Lin. Input forces estimation of beam structures by an inverse method. *Journal of Sound and Vibration*, 259(2):387–407, January 2003.

[2] Pan-Chio Tuan, Ching-China Ji, Li-Wei Fong, and Wen-Tang Huang. An input estimation approach to on-line two-dimensional inverse heat conduction problems. *Numerical Heat Transfer, Part B: Fundamentals*, 29(3):345–363, April 1996.

[3] X. Ma, N.K. Poulsen, and H. Bindner. Estimation of wind speed in connection to a wind turbine. Technical Report IMM-1995-26, Informatics and Mathematical Modelling, Technical University of Denmark, DTU, December 1995.

[4] K.Z. Østergaard, P. Brath, and J. Stoustrup. Estimation of effective wind speed. *Journal of Physics: Conference Series*, 75, 2007.

[5] B. Boukhezzar, H. Siguerdidjane, and M. Hand. Nonlinear control of variable speed wind turbines for load reduction and power optimization. In *44th AIAA Aerospace Sciences Meeting and Exhibit*, pages 602–615, Reno, NV, January 2006.

[6] Julian Ehlers, Amadou Diop, and Henrik Bindner. Sensor selection and state estimation for wind turbine controls. In *45th AIAA Aerospace Sciences Meeting and Exhibit*, Reno, NV, January 2007.

[7] NWTC Design Codes. FAST by Jason Jonkman. http://wind.nrel.gov/designcodes/simulators/fast/, August 12, 2005. Accessed 21-May-2008.

[8] John L. Crassidis and John L. Junkins. *Optimal Estimation of Dynamic Systems*. Chapman & Hall/CRC, 2004.

[9] NWTC Design Codes. TurbSim by Neil Kelley, Bonnie Jonkman. http://wind.nrel.gov/designcodes/preprocessors/turbsim/, April 4, 2008. Accessed 28-May-2008.